Virology 269, 325–334 (2000)
doi:10.1006/viro.2000.0228, available online at http://www.idealibrary.com on IDEAL®

The Cytoplasmic Tails of the Influenza Virus Spike Glycoproteins Are Required for Normal Genome Packaging

Jie Zhang,* George P. Leser,* Andrew Pekosz,† and Robert A. Lamb*,†,[1]

*Department of Biochemistry, Molecular Biology, and Cell Biology, and †Howard Hughes Medical Institute, Northwestern University, Evanston, Illinois 60208-3500

Received December 10, 1999; returned to author for revision January 18, 2000; accepted February 2, 2000

Deletion of the cytoplasmic tails of the influenza A virus spike glycoproteins, hemagglutinin (HA) and neuraminidase (NA), has previously been shown to result in markedly defective virion morphogenesis (Jin *et al.,* 1997, *EMBO J.* 16, 1236–1247). We have found that influenza A virus preparations lacking the HA and NA cytoplasmic tails (HAt−/NAt−) have a reduced vRNA to protein content, contain an increase in cellular RNA contaminants, and exhibit increased resistance to ultraviolet (UV) inactivation. There is also a direct correlation between abnormal virion morphology and reduced infectivity. The data suggest that the HAt−/NAt− virion population contains a broader range of number of packaged RNA segments than wild-type (wt) virus. Sucrose gradient centrifugation analysis indicated the presence of a subpopulation of virions with pronounced deformation in virion morphology and reduced infectivity. The role of the HA and NA cytoplasmic tails was examined further by using a trans-complementation assay and it was found that expression of wt HA and NA from cDNAs followed by HAt−/NAt− virus infection caused the formation of a pseudotype virus with wt sedimentation properties. Taken together the data indicate that the HA and NA cytoplasmic tails affect not only virion morphology but also proper genome packaging.

INTRODUCTION

The mechanism by which influenza A virus assembles and buds from the plasma membrane is not well understood. The influenza virus envelope contains two major integral membrane glycoproteins, hemagglutinin (HA) and neuraminidase (NA) and, in much lower abundance, the M_2 ion channel protein. Contained within the influenza virus envelope are the viral matrix (M_1) protein and the eight virus RNA segments found as helical ribonucleoprotein capsids (RNPs; reviewed in Lamb and Krug, 1996). It has been widely viewed that interactions between the cytoplasmic tails of the viral integral membrane proteins and the internal components of the virion provide the necessary molecular information for formation of the budding particle.

The HA C-terminal cytoplasmic tail contains 10 or 11 amino acid residues (depending on HA subtype), working under the assumption that the charged residue adjacent to the hydrophobic transmembrane (TM) domain delineates the boundary of the domain: these residues are highly conserved among the 15 HA subtypes (Nobusawa *et al.,* 1991). The six residues comprising the predicted NA cytoplasmic tail are also highly conserved among the nine NA subtypes (Colman, 1989). Given the mutation rate of the influenza virus RNA genome, this sequence conservation suggests an important function for the HA and NA cytoplasmic tails.

Reverse genetics procedures have been used to generate novel influenza viruses that lack either the cytoplasmic tail of HA (HAt−/NA) (Jin *et al.,* 1994, 1996) or the cytoplasmic tail of NA (HA/NAt−) (Garcia-Sastre and Palese, 1995; Mitnaul *et al.,* 1996). The HAt−/NA virus incorporated HA and other virion polypeptides in an amount similar to wild-type (wt) (HA/NA) virus, and the HAt−/NA virions had a spherical morphology similar to wt virus grown in eggs. However, the HAt−/NA virions exhibited a somewhat lower budding efficiency and were slightly less infectious than wt virus (Jin *et al.,* 1994, 1997). The HA/NAt− virus had 1–2 log lower infectivity in tissue culture (Garcia-Sastre and Palese, 1995; Mitnaul *et al.,* 1996; Jin *et al.,* 1997) and exhibited a tendency to form more filamentous than spherical particles (Mitnaul *et al.,* 1996; Jin *et al.,* 1997). Analysis of the double mutant HAt−/NAt− virus showed that this virus had a 1 log reduction in infectivity in eggs and an approximately 3 log lower infectivity in MDCK cells as compared with wt virus. HAt−/NAt− virions, for an equivalent amount of HA, showed reduced incorporation of NA and M_1 proteins. As judged by electron microscopy, the HAt−/NAt− virions exhibited greatly altered morphology: vastly extended lengths and irregular diameters (Jin *et al.,* 1997). From these observations of properties of HAt−/NAt, HA/

[1] To whom correspondence and reprints requests should be addressed at Northwestern University, Department of Biochemistry, Molecular Biology, and Cell Biology, 2153 North Campus Drive, Evanston, IL 60208-3500. Fax: (847) 491-2467. E-mail: ralamb@nwu.edu.

0042-6822/00 $35.00

NAt−, and HAt−/NAt− virions, we proposed a model in which, for the normal budding of influenza virus, the requirements of the HA and NA cytoplasmic tail interactions with an internal component of the virion (most likely the M_1 protein) are so critical for normal budding that these cytoplasmic tail interactions are redundant (Jin *et al.,* 1997).

We have studied further properties of the HAt−/NAt− virus to investigate the impact of HA and NA cytoplasmic tail deletions on virus genome packaging and assembly and to determine whether particles with greatly altered morphology are as infectious as the spherical particles. Altered virion morphology was found to correlate with the reduced infectivity of the HAt−/NAt− virus. The HAt−/NAt− virion preparations contained less viral RNA in comparison with the amount of viral protein, but more cellular RNA contaminants. HAt−/NAt− virions also exhibited a higher particle-to-plaque-forming unit (PFU) ratio and were more resistant to UV light inactivation. Velocity sucrose sedimentation analysis of HAt−/NAt− virions showed a particle distribution different from that of wt HA/NA virions, but could be restored by expression in *trans* of the wt HA and NA proteins in HAt−/NAt− virus-infected cells. Taken together these data suggest the deletions of both HA and NA cytoplasmic tails affects not only virion morphology but also proper genome packaging.

RESULTS

RNA composition of HAt−/NAt− virus

The effect of HA and NA cytoplasmic tail deletions on viral genome packaging was analyzed by extracting RNA from equivalent amounts (500 μg protein) of purified HAt−/NAt− and HA/NA virions. RNA species were separated by electrophoresis on polyacrylamide gels and detected using ethidium bromide staining. Although the overall segment-to-segment ratio was not grossly altered, the total amount of RNA present in HAt−/NAt− virus was reduced in comparison with that of HA/NA virus (Fig. 1A). An extra approximately 1900-nucleotide RNA species was observed for HAt−/NAt− virus and it was shown to be 18S ribosomal RNA (rRNA) by Northern blot analysis (Fig. 1B). Quantification of the RNA content of HAt−/NAt− and HA/NA viruses using probes specific for influenza virus RNA segments encoding PA, PB1, PB2, or M proteins indicated the RNA segment-to-protein ratio was reduced in the HAt−/NAt− virus by 3.7-fold (PA, PB1, and PB2 segments) or five-fold when compared with HA/NA virus. Surprisingly, 28S rRNA was not detected by ethidium bromide staining in the HAt−/NAt− virus. Northern blot analysis of virion RNA and host cell cytoplasmic RNA, using a probe specific for 28S rRNA, showed only barely detectable amounts of 28S rRNA in the virion preparations (data not shown). Nonetheless, this could be an underestimate of the amount of 28S rRNA, as this rRNA species migrates diffusely and transfers to blots inefficiently. The presence of 40S ribosomal subunits, containing 18S RNA, within HAt−/NAt− virions has not been verified and their presence in the virion preparation could be the result of contaminating vesicles. However, examination of the virions by electron microscopy did not show a large number of contaminating vesicles (see below). The reduced viral genome RNA content suggests a reduced specificity and/or efficiency in viral genome packaging for the HAt−/NAt− virus.

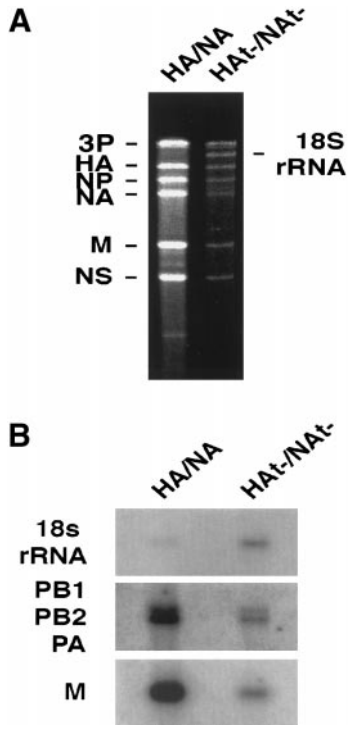

FIG. 1. RNA composition of HA/NA and HAt−/NAt− viruses. (A) RNA was extracted from purified HA/NA and HAt−/NAt− virions (500 μg total protein), and vRNAs analyzed by gel electrophoresis with a 4% polyacrylamide gel containing 9 M urea. RNA was detected by staining with ethidium bromide. (B) Northern blot analysis of virion RNA. Total RNA was extracted from purified virions, separated on 1% agarose/formamide gels, and blotted to a nylon membrane. The membranes were hybridized with [^{32}P]-labeled riboprobes specific for 18S ribosomal RNA, influenza virus RNA segments PA, PB1, PB2, or influenza virus RNA segment M.

UV light inactivation of HAt−/NAt− virus

The lower vRNA-to-protein ratio of the HAt−/NAt− virus as compared with wt HA/NA virus could be a result of either an increased amount of protein present in each infectious virus particle or the production of a large number of virions containing an incomplete set of RNA segments. To distinguish between these two possibilities, ultraviolet (UV) inactivation was used to test the extent of multiplicity of reactivation for each virus (Luria and Dulbecco, 1949; Barry, 1961). Approximately 10^6 PFU of HA/NA and HAt−/NAt− viruses were exposed to 0, 5,

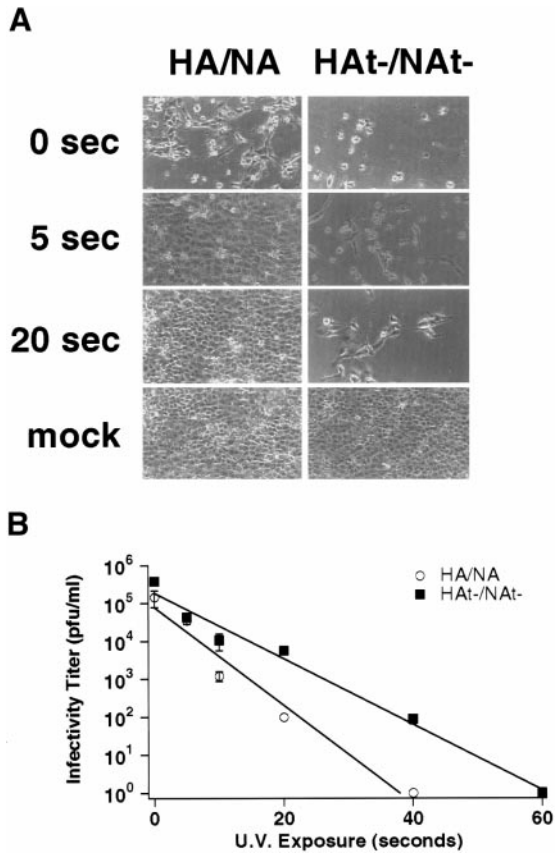

FIG. 2. Multiplicity reactivation and UV light inactivation profiles of the HA/NA and HAt−/NAt− viruses. (A) A 100-μl sample containing 10^6 plaque-forming units (PFUs) of egg-grown HA/NA or HAt−/NAt− viruses was exposed to UV light for the periods indicated. Approximately 10^5 MDCK cells were infected with the irradiated viruses and the cytopathic effect examined at 24 hpi. (B) Egg-grown HA/NA and HAt−/NAt− viruses were exposed to UV light for the indicated times and the infectious virus titer was determined by plaque assay on MDCK cells.

or 20 s of UV irradiation and the viruses used to infect confluent monolayers of MDCK cells ($\sim 10^5$ cells). For nonirradiated viruses, massive cytopathic effect (CPE) and cell loss was observed after 24-h incubation (Fig. 2A). For wt HA/NA virus irradiated for 5 or 20 s, no obvious signs of CPE were observed (Fig. 2A). In contrast, HAt−/NAt− virus irradiated for 5 or 20 s still produced massive CPE and cell loss. These data indicate HAt−/NAt− virus is less sensitive to UV light inactivation. This is likely the result of the presence of a large number of noninfectious particles in the HAt−/NAt− virus population containing random numbers of RNA segments, which resulted in multiplicity reactivation (Luria and Dulbecco, 1949; Barry, 1961).

A separate approach to examining altered genome RNA segment composition in infectious HA/NA and HAt−/NAt− particles was to examine directly the sensitivity to UV light inactivation by determining residual infectivity by plaque assay. The HAt−/NAt− virus was found to require a greater dose of UV radiation for equivalent inactivation (Fig. 2B), as compared with wt HA/NA virus. The decreased sensitivity of HAt−/NAt− infectious particles to UV light inactivation most likely results from the packaging of more than a full complement of RNA segments in some infectious particles of HAt−/NAt− virus. Formally, however, the possibility also exists that the presence of a greater number of large noninfectious particles may absorb or scatter some of the incident energy.

Sucrose gradient centrifugation analysis

To investigate the relationship between virion morphology and infectivity, [^{35}S]-labeled virions grown in MDCK cells were analyzed by ultracentrifugation on 20–50% sucrose gradients and the gradient fractions assayed for hemagglutination (HA), infectivity by plaque assay, and polypeptide composition. As shown in Fig. 3A, whereas fraction 14 was the peak fraction of viral protein for HA/NA virus, the peak fraction for HAt−/NAt− viral protein was shifted to fraction 12. The pattern of M_1 protein found in each gradient fraction coincided with the distribution of physical particles as determined by hemagglutination assay (Fig. 3B), confirming the broader distribution and shift in peak fractions across the gradient for HAt−/NAt− virus as compared with HA/NA virus. When the distribution of infectious particles across the gradient was determined by plaque assay, the peak of infectivity for both HAt−/NAt− and wt HA/NA virus was found in fraction 14. Thus, whereas for wt HA/NA virus the peak of physical particles and infectious particles coincided, for HAt−/NAt− virus the peak of physical particles was shifted from that of the infectious particles, suggesting the presence of a subpopulation of HAt−/NAt− virus particles of lower infectivity, which can be separated from the more infectious virus population. Examination of egg-grown HA/NA and HAt−/NAt− showed a sedimentation pattern and infectivity pattern very similar to that found for MDCK-grown virions (data not shown).

The density of [^{35}S]-labeled HA/NA and HAt−/NAt− virus particles grown in MDCK cells was determined by equilibrium sucrose gradient ultracentrifugation. Peak radioactivity was determined by scintillation counting and the density of each gradient fraction determined by weighing 100 μl of each fraction. The peak fraction for both viruses was fraction 28 (1.18 g/ml) (Fig. 3C). Taken together the data shown in Fig. 3 suggests that for HAt−/NAt− there is a subpopulation of HAt−/NAt− particles which are less infectious and can be separated by velocity gradient centrifugation from the infectious virus subpopulation.

Morphology of HAt−/NAt− virus subpopulations

Wt HA/NA and HAt−/NAt− were grown in eggs, and virions were purified and examined by electron micros-

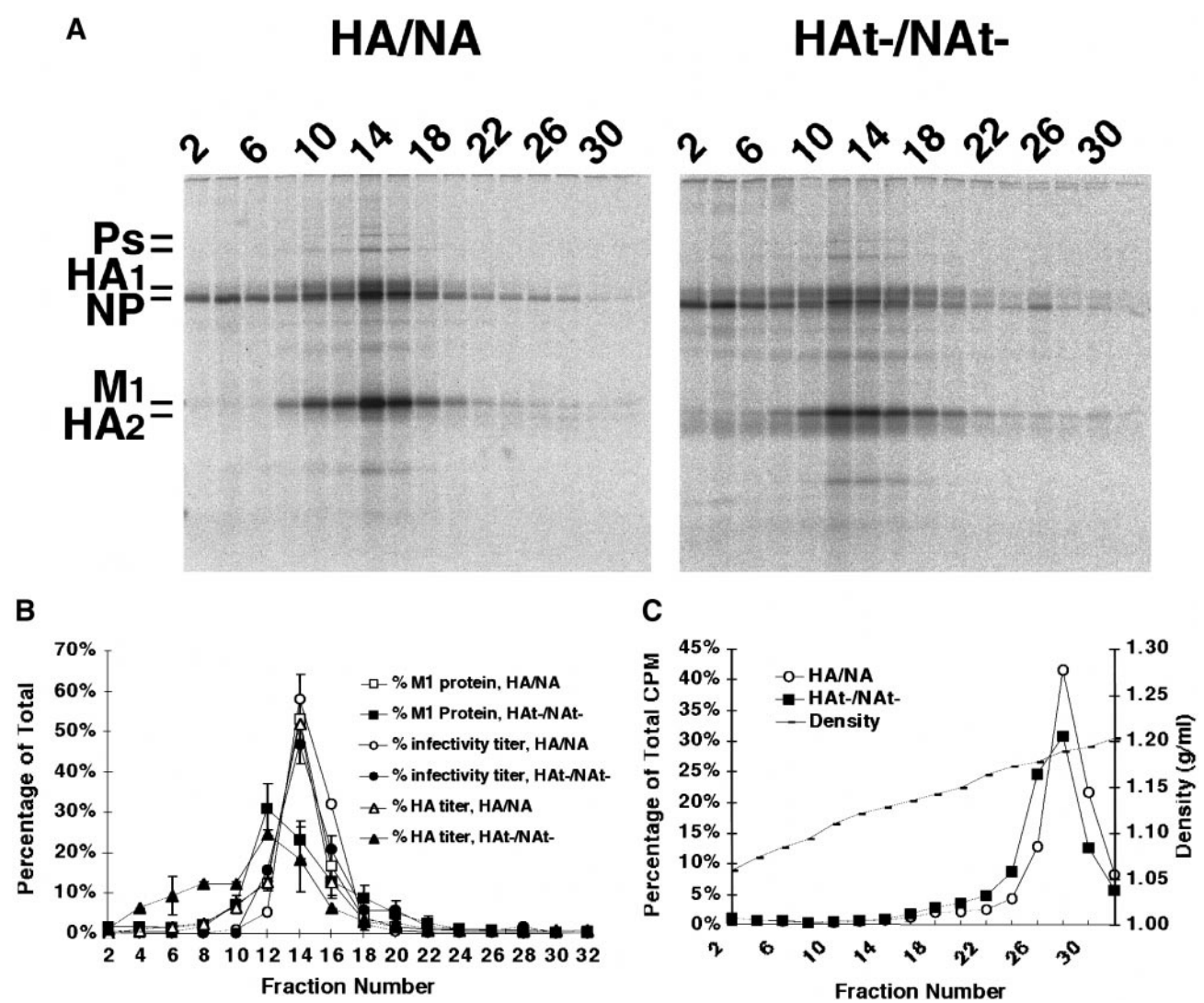

FIG. 3. Sucrose gradient centrifugation of HA/NA and HAt−/NAt− viruses. (A) Velocity sedimentation of HA/NA and HAt−/NAt− virions. MDCK cells were infected with HA/NA or HAt−/NAt− viruses and the cells metabolically labeled with [^{35}S]Promix for 12 h. The medium was harvested, clarified by low-speed centrifugation, and virions pelleted by ultracentrifugation. The virions were resuspended in NTE buffer, overlaid onto a linear 20–50% sucrose gradient, and centrifuged in a Beckman SW41 rotor (130,000 *g*, 1 h, 4°C). The gradients were fractionated from the top. Virions were precipitated using TCA (final concentration 10%) and polypeptides in each fraction analyzed by SDS–PAGE on 15% acrylamide gels. (B) Physical particle and infectious particle profiles of HA/NA and HAt−/NAt− virion populations separated by velocity sucrose gradient centrifugation. The amount of M_1 protein in each fraction was quantified by using a Fuji BioImager 1000. The HA and infectivity titers of the fractions were also determined by hemagglutination assay and plaque assay. The data from (A) and (B) are from two independent experiments. (C) Equilibrium sucrose gradient centrifugation of [^{35}S]-labeled HA/NA and HAt−/NAt− viruses grown in MDCK cells. Pelleted virus was resuspended in NTE, overlaid onto a linear 20–50% sucrose gradient, and centrifuged in an SW41 rotor (130,000 *g*, 18 h, 4°C). The amount of radioactivity in each fraction was determined by scintillation counting. The density of each fraction was determined by weighing a 100-μl sample of each fraction.

copy. As found previously, wt HA/NA virions were largely spherical (~100 nm diameter), whereas HAt−/NAt− virions were heterogeneous in shape, ranging from some spherical particles to a majority of particles having vastly extended diameters and lengths (1–2 μM length; data not shown) (Jin *et al.,* 1997). MDCK cell-grown HA/NA and HAt−/NAt− virions retained their respective morphologies and were very similar to egg-grown virus in both the form and extent of the heterogeneity observed in the electron microscope (data not shown). MDCK-grown HA/NA and HAt−/NAt− viruses also exhibited sedimentation patterns similar to that of egg-grown virus, as judged by the HA titer distributions (data not shown). Thus, because of the higher virus yield egg-grown virions were used. Polystyrene beads were used in the diluted virions as an internal standard to permit comparison of the relative virus concentration when viewed by the electron microscope. The HAt−/NAt− population had an average of 14.6 ± 5.3 particles per field of view (n = 19) and an infectious titer of 5×10^7 PFU/ml (Table 1). The HA/NA virions averaged 26.3 ± 8.0 particles per field of view (n = 20) with a titer of 3.05×10^8 PFU/ml (Table 1).

TABLE 1

Quantification of the Physical and Infectious Particles of the HA/NA and HAt−/NAt− Viruses

	Bead number/field	Wt shaped particles/field	Elongated particles/field	Total number of particles/field	Infectivity (PFU/ml)
HA/NA[a]	10.2 ± 3.2	ND	ND	26.3 ± 8.0	3.05×10^8
HAt−/NAt−[b]	10.9 ± 3.1	ND	ND	14.6 ± 5.3	5×10^7
HAt−/NAt− fractions 10–12[c]	11.3 ± 4.2	18.6 ± 4.9	73 ± 12.0	91.5 ± 14.7	8.4×10^4
HAt−/NAt− fractions 13–14[d]	9.6 ± 3.3	7.7 ± 2.7	15 ± 3.3	22.8 ± 4.8	1.4×10^5

Note. Fields of view: [a]$n = 19$; [b]$n = 20$; [c]$n = 16$; [d]$n = 17$.

Thus, there were approximately threefold more noninfectious particles in the HAt−/NAt− population as compared with the HA/NA population (Table 2). To examine whether the HAt−/NAt− virions that sedimented in the peak of physical particles (fractions 10–12) in Fig. 3 had an altered morphology from those that sedimented in the peak of infectious particles (fractions 13–14), the particles were examined by electron microscopy. Fractions 10 to 12, containing the peak of physical particles, had an average of 91.5 ± 14.7 particles per field ($n = 16$) compared with 22.8 ± 4.8 particles for fractions 13 and 14 ($n = 17$), the peak fractions of infectivity. In addition to the greater number of physical particles, fractions 10–12 also contained approximately 73 ± 12.0 heterogeneously shaped particles as compared with 15.0 ± 3.3 heterogeneous particles for fractions 13–14 (Fig. 4, Table 1). The infectious titers were 8.4×10^4 PFU/ml for fractions 10–12 and 1.4×10^5 PFU/ml for fractions 13–14. Therefore, fractions 10–12, containing the peak of physical particles, not only contained four-fold more particles than fractions 13–14 (Fig. 4; Table 1), but this fraction also contained approximately twice the number of heterogeneously shaped particles versus wt particles as compared with fractions 13–14 (Fig. 4; Table 2). The relative ratio of physical particles to infectious particles for fractions 10–12 was about six-fold higher than for HAt−/NAt− virions in fractions 13–14. Thus, the physical particle peak fractions (10–12) represent a major subpopulation of HAt−/NAt− virus particles that contains a much greater percentage of particles with deformed shape and lower overall infectivity.

TABLE 2

Quantification of the EM Data of HAt−/NAt− Virions Separated on Sucrose Gradients

	Relative particle number[a]	Deformed/wt particles	Relative physical/infectious particle number[b]
HAt−/NAt− fractions 10–12	4	3.92	5.6
HAt−/NAt− fractions 13–14	1	1.96	1

[a] Relative particle number is the number of total particles when normalized to that of fractions 13–14.

[b] Relative physical/infectious particle number is the ratio of physical/infectious particles when normalized to that of fractions 13–14.

Pseudotyping HAt−/NAt− virions with wt HA and NA glycoproteins partially restores the virus sedimentation profile

To provide additional evidence that the HA and NA cytoplasmic tails are involved with altered virion physical properties, we investigated the ability of wt HA and NA to pseudotype HAt−/NAt− virions by expressing HA and NA from cDNAs in HAt−/NAt− infected cells. As a high efficiency of transfection was sought, the experiment was performed using BHK cells. However, a drawback of BHK cells is that they produce only low levels of budding virus. BHK cells were transfected with plasmids expressing influenza virus HA and NA or a control plasmid expressing the influenza C virus hemagglutinin, esterase, fusion (HEF) protein. The transfection efficiency, as determined by flow cytometry, was 70% for HA and NA and 73% for HEF.

At 22 h posttransfection, the indicated cultures were infected with wt HA/NA or HAt−/NAt− viruses, metabolically labeled with [^{35}S]Promix at 3 h postinfection (hpi), and at 24 hpi supernatants were collected and subjected to velocity centrifugation on sucrose gradients. The polypeptide profile of the gradient fractions is shown in Figs. 5A–5D. For virions grown in BHK cells the wt HA/NA peak (Fig. 5A) was found in fractions 11–15, whereas the HAt−/NAt− virus was found broadly distributed but with a peak in fractions 17–21 (Fig. 5B). The sedimentation pattern for HAt−/NAt− virus grown in BHK cells is different from that observed for HAt−/NAt− virus grown in MDCK cells or eggs (e.g., Fig. 3). Examination of HAt−/NAt− virions grown in BHK cells by electron microscopy was hindered by the paucity of released virions, although for the limited number of particles examined it was found that the HAt−/NAt− virions were still deformed, but they tended to be more homogenous than when compared with HAt−/NAt− grown in mock-transfected BHK cells (data not shown).

When wt HA and NA were expressed from cDNA in HAt−/NAt− virus-infected BHK cells, there was a shift in the sedimentation pattern of the released virions from

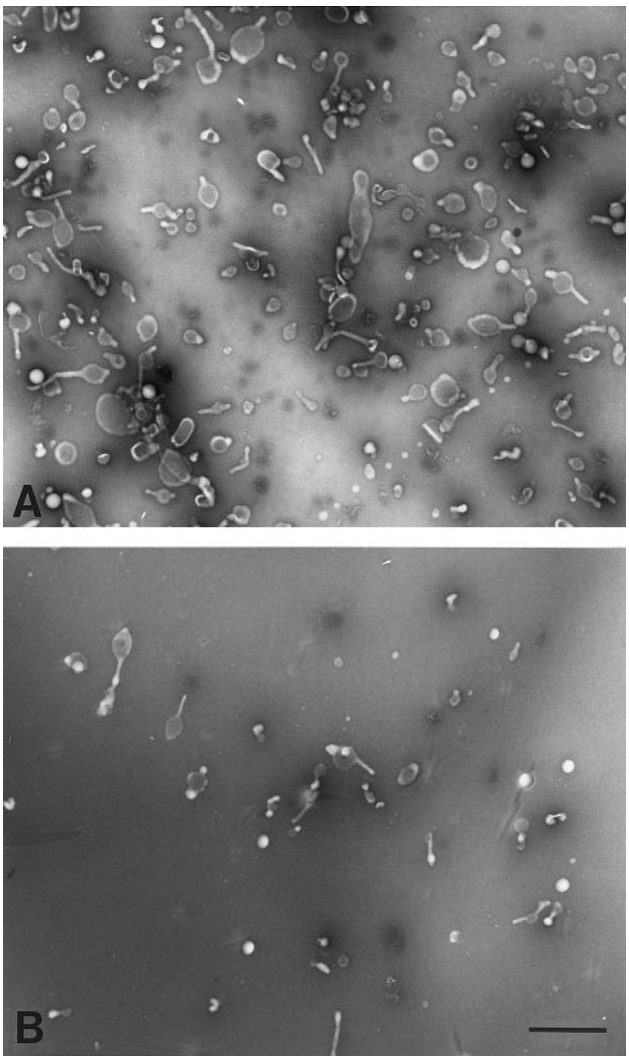

FIG. 4. Morphology of the HAt−/NAt− virions contained in the peak fractions of physical and infectious particles. HAt−/NAt− virus was grown in embryonated eggs and purified as described under Materials and Methods. The virions were analyzed by velocity sedimentation as described in the legend to Fig. 3. Fractions 10–12 (A) and 13–14 (B) were pooled, pelleted, resuspended in NTE buffer, and diluted in NTE containing a known concentration of polystyrene beads and absorption of the mixture onto electron microscopy grids. Specimens were negatively stained with phosphotungstic acid and examined by electron microscopy. The average number of beads counted per field for fractions 10–12 was 11.3 ± 4.2 (n = 16), while the average was 9.6 ± 3.3 (n = 17) for fractions 13–14. Magnification, 19,000×. Bar = 500 nm.

fractions 17–21 to fractions 13–19 (Figs. 5C and 5F). Expression of HEF in HAt−/NAt− virus-infected BHK cells had no effect on the sedimentation pattern of the released virions (Fig. 5D). To show that wt HA and NA were incorporated into HAt−/NAt− virions, transfected BHK cells were metabolically labeled prior to infection with HAt−/NAt− virus and released virions were subjected to velocity sedimentation on sucrose gradients. To detect the pseudotyped HA and NA, the polypeptides in each fraction were immunoprecipitated with HA- or NA-specific sera. To facilitate identification of polypeptide species on gels, samples were treated with peptide N-glycanase prior to SDS–PAGE. The wt HA and NA proteins were found to sediment predominantly in fractions 11–15 (Fig. 5E), analogous to the sedimentation pattern of wt HA/NA (Fig. 5A) and the pseudotyped HAt−/NAt− virus (Fig. 5C). Because there was no change in the virion profile between mock and HEF-expressing BHK cells, we did not look for incorporation of HEF into HAt−/NAt− virus particles. The low overall infectivity of HAt−/NAt− infected BHK cell supernatants precluded us from determining whether there was an increase in infectivity in the *trans*-complemented virus population as compared with control HAt−/NAt− virus. Nonetheless, these data indicate that incorporation of wt HA and NA proteins into HAt−/NAt− virions restores wt virus-like sedimentation properties to HAt−/NAt− virus.

DISCUSSION

The HA and NA cytoplasmic tail-deleted HAt−/NAt− virus exhibits a grossly altered morphology with a large proportion of pleomorphic virions of extended diameters and lengths (Jin *et al.,* 1997). As shown here, the HAt−/NAt− virion population contains a reduced total viral RNA content. Two lines of evidence suggest that the RNA composition of HAt−/NAt− virions is different from that of wt virus. First, a longer period of UV light inactivation is required to prevent HAt−/NAt− virus from causing cytopathic effects as compared with wt virus. Multiplicity reactivation is the regaining of infectivity by infection of cells with more than one particle containing less than a full genome complement (Luria and Dulbecco, 1949). Thus, the data shown in Fig. 2A suggest that for an equivalent infectious virus titer, HAt−/NAt− virus contains more noninfectious particles (i.e., particles with less than eight RNA segments) than wt virus. Second, the infectivity (as measured by plaque assay) of HAt−/NAt− virus was more resistant to a given UV light inactivation dosage than wt virus. These data suggest that the infectious HAt−/NAt− virus population is likely to contain more than a full complement of eight RNA segments as compared with infectious wt virus. Thus, resistance to UV light inactivation in this case would occur through an irradiated RNA segment being complemented by an equivalent, nonirradiated RNA segment in the same virion. Taken together the two UV irradiation experiments suggest that HAt−/NAt− virus particles are likely to contain a much broader distribution in the number of RNA segments packaged than wt virus. The fractionation of HAt−/NAt− particles by velocity sedimentation on sucrose density gradients and the determination of the physical and infectious particle profiles, coupled with examination of the particle morphology, indicates a tight correlation between reduced infectivity and altered morphology. Despite the larger size of HAt−/NAt− virions grown in MDCK cells than wt virus, HAt−/NAt− particles

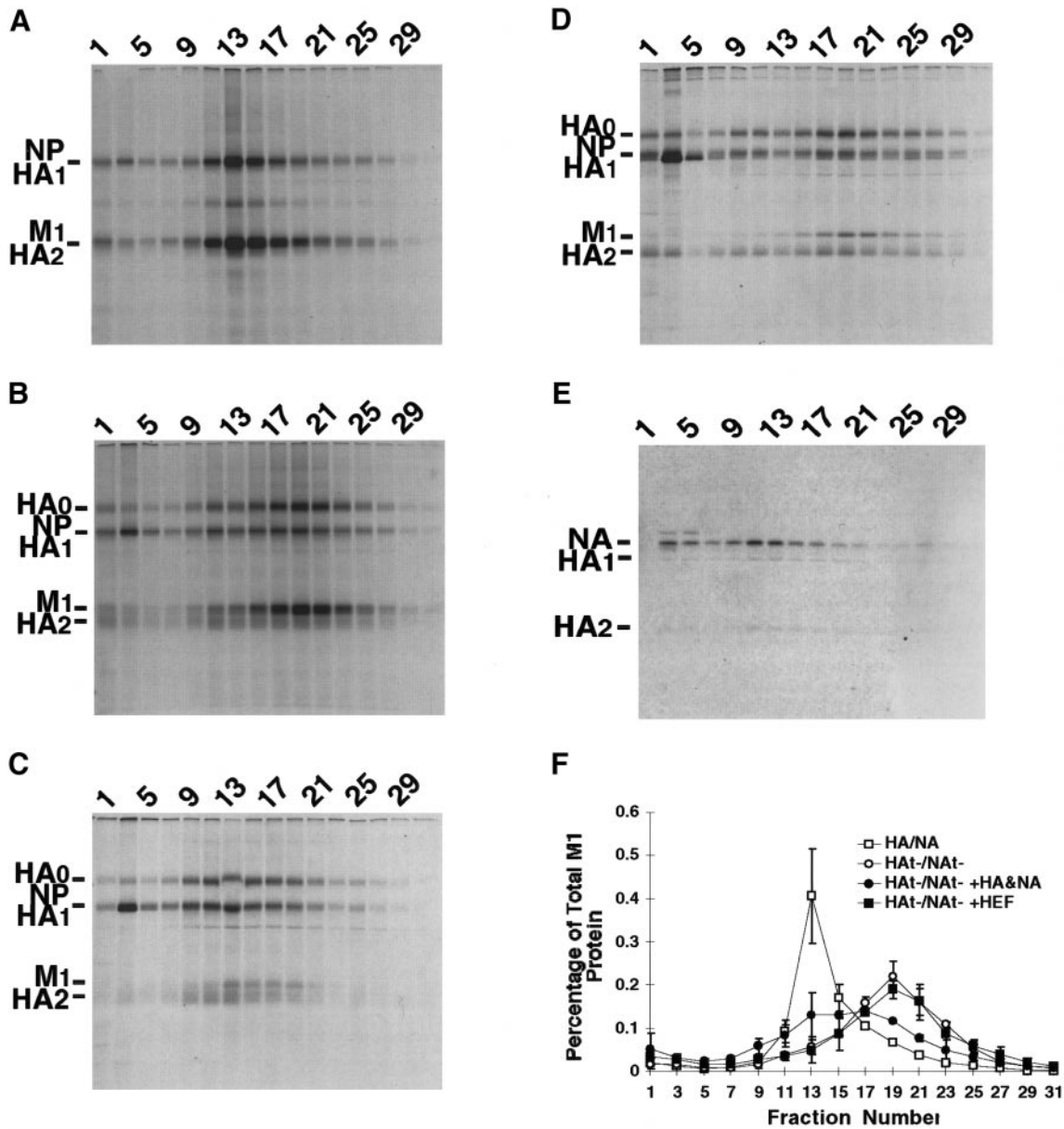

FIG. 5. Pseudotyping of the HAt−/NAt− virus with wt HA and NA proteins. BHK cells in 10-cm-diameter dishes were transiently transfected with plasmids expressing wt HA and wt NA or influenza C virus HEF glycoprotein. At 22 h posttransfection cells were infected with either wt HA/NA virus or HAt−/NAt− virus. At 3 h postinfection (hpi) cells were labeled with DMEM containing [^{35}S]Promix (100 μCi/ml). Twenty four hpi the cell supernatant was harvested and subjected to velocity centrifugation on sucrose gradients as described in the legend to Fig. 3. Polypeptides in each fraction were analyzed by SDS–PAGE on 15% acrylamide gels. The panels show the polypeptide pattern across gradients of virions obtained from: (A) mock-transfected, HA/NA virus-infected cells; (B) mock-transfected, HAt−/NAt− virus-infected cells; (C) cells transiently expressing wt HA and wt NA and infected with HAt−/NAt− virus; (D) cells transiently expressing influenza C virus HEF glycoprotein and infected with HAt−/NAt− virus. (E) Incorporation of wt HA and wt NA into HAt−/NAt− virions. BHK cells were transiently transfected with plasmids expressing wt HA and wt NA glycoproteins and the cultures were labeled with [^{35}S]Promix from 18 to 22 hpi. The labeling medium was removed and cells were infected with HAt−/NAt− virus. At 24 hpi the medium was harvested and virions subjected to velocity centrifugation on sucrose gradients as described earlier. The gradient fractions were diluted with an equal volume of 2× RIPA buffer and HA and NA immunoprecipitated using HA and NA-specific sera (Jin *et al.,* 1997). To facilitate electrophoretic separation of HA and NA, immunoprecipitated polypeptides were digested with peptide N-glycanase as described previously (Paterson and Lamb, 1993). Polypeptides were analyzed by SDS–PAGE using 15% acrylamide gels. (F) The amount of M_1 protein in each fraction of panels (A)–(D) is plotted as a percentage of the total M_1 protein.

are found in similar density fractions (Fig. 3) under equilibrium centrifugation conditions. This is consistent with a reduced RNA-to-lipid/protein ratio in the HAt−/NAt− particles because at 1% RNA by weight in wt influenza virus, the RNA contributes little to the total mass. Thus, the deletions in the cytoplasmic tails of HA and NA not only affect virion morphology but lead to reduced infectivity, most likely as a result of inefficient packaging of

vRNP segments. The inefficient budding process of HAt−/NAt− virus may also lead to the presence of 18S ribosomal RNA, presumably as 40S ribosomal subunits, associated with virions. It is possible that the reduced infectivity of HAt−/NAt− is also the result of defects in virus entry into cells; however, it is known that HAt− causes cell-cell fusion in a manner nearly indistinguishable from that of wt HA (Jin *et al.,* 1996; Melikyan *et al.,* 1997).

Filamentous forms of influenza A virus have been observed in clinical isolates (Burnet and Lind, 1957; Ada *et al.,* 1958; Choppin *et al.,* 1960, 1961; Kilbourne and Murphy, 1960) and for the A/Udorn/72 virus grown in specific cell types (Roberts *et al.,* 1998). These filamentous (1–2 μM length) particles possess a uniform diameter and are often more infectious than the wt spherical particles (Kilbourne and Murphy, 1960). In contrast, the HA and NA cytoplasmic tail-deficient HAt−/NAt− virus is vastly pleomorphic in diameter and length. Influenza virus grown in eggs treated with vitamin A alcohol have a grossly altered morphology with a large proportion of pleomorphic virions of extended diameters and lengths (Blough, 1963) similar to that of HAt−/NAt− virions, although the mechanism of action of vitamin A alcohol is not known.

A growing body of data suggests that viral glycoprotein cytoplasmic tails provide specificity in the assembly process and promote efficient budding. Both rabies virus and VSV recombinants containing deletions of the G protein cytoplasmic tail were found to bud inefficiently, and 5- to 10-fold reductions in the amounts of viral proteins released into the supernatants of virus-infected cells were reported (Mebatsion *et al.,* 1996; Schnell *et al.,* 1998). Recombinant rabies virions possessing a G protein with a truncated cytoplasmic tail contained less G protein as compared with other viral proteins (Mebatsion *et al.,* 1996), suggesting that specific incorporation of G protein into virions depends on the presence of the G protein cytoplasmic tail. Recombinant measles virions containing alterations to the cytoplasmic tails of its spike glycoproteins, hemagglutinin (H) or fusion protein (F), also contained reduced amounts of the altered glycoproteins (Cathomen *et al.,* 1998). Recombinant paramyxovirus SV5 containing deletions to the hemagglutinin-neuraminidase (HN) glycoprotein cytoplasmic tail were shown to be replication-impaired and the release of progeny virion particles from cells was inefficient as compared with wt virus (Schmitt *et al.,* 1999). Furthermore, accumulation of viral proteins at presumed budding sites on the plasma membranes of infected cells was disrupted by HN cytoplasmic tail truncations (Schmitt *et al.,* 1999). For the measles and SV5 glycoprotein tail-deletion mutants, an increase in the nonspecific incorporation of cellular proteins into these virions was also observed, further supporting the view that the glycoprotein cytoplasmic tails contribute to specificity in virus assembly. Interestingly for influenza viruses that lack the HA or NA or both HA and NA cytoplasmic tails, there is not an obvious increase in host cell proteins in the purified virion (Jin *et al.,* 1997).

Previously, in considering the inefficient assembly of paramyxoviruses that lack glycoprotein cytoplasmic tails or the matrix protein we argued for the need to distinguish bona fide viruses from "gollum" viruses, infectious material that has been passively assembled and that lacks a genetic "soul" (resulting from the introduced mutation), necessary for efficient budding (Schmitt *et al.,* 1999). For the HAt−/NAt− virus it is clear from the virus titers that the production of particles is occurring vastly more efficiently that the endogenous rate of vesicle blebbing (Rolls *et al.,* 1994). Nonetheless, for HAt−/NAt− virus the assembly process is seriously disrupted, leading to gross deformities in the shape and size of released virions and abnormal packaging of RNA segments. Thus, for influenza virus the conserved HA and NA cytoplasmic tails are extremely important for proper virus assembly.

MATERIALS AND METHODS

Cells and viruses

Madin-Darby canine kidney (MDCK) and baby hamster kidney cells (BHK) were maintained in Dulbecco's modified Eagle's medium (DMEM) supplemented with 10% fetal bovine serum. The influenza viruses used in this study, HA/NA, HAt−/NA, HA/NAt−, and HAt−/NAt−, have been described previously (Jin *et al.,* 1997): t− indicates a cytoplasmic tail deleted from the indicated protein. HAt−, which lacks the HA cytoplasmic tail (by insertion in the cDNA of three consecutive stop codons), also contains a substitution of HA cysteine residue 555 for methionine and this double mutation had at one time been designated Mtr− (Jin *et al.,* 1996). NAt− contains a deletion of the five N-terminal residues of NA occurring after the initiation methionine codon (Garcia-Sastre and Palese, 1995). HA was from A/Udorn/1/72 (H3 subtype) and NA (N1 subtype), as well as the remainder of the viral RNA segments, from A/WSN/33 (Jin *et al.,* 1997). Plaque assays were performed as described previously (Paterson and Lamb, 1993).

Virus purification

Viruses were grown in 11-day embryonated eggs, MDCK cells, or BHK cells. Allantoic fluid or tissue culture supernatants were clarified by centrifugation at 2000 *g* for 20 min. The virus particles were subsequently pelleted by centrifugation in a Beckman SW41 ultracentrifuge rotor (210,000 *g*, 1 h, 4°C). Virus pellets were resuspended in NTE buffer (10 mM Tris [pH 7.4], 100 mM NaCl, 1 mM EDTA) and protein concentration was determined using a BCA assay (Pierce Chemical Co., Rockford, IL).

Viral RNA extraction and Northern blot analysis

For viral RNA extraction, purified virions (500 μg) were disrupted with 0.5% sodium dodecyl sulfate (SDS) and digested with 50 μg/ml proteinase K at 45°C for 1 h, followed by phenol/chloroform extraction and ethanol precipitation (Ausubel *et al.,* 1994). The viral RNA was analyzed by electrophoresis on 4% polyacrylamide gels containing 9 M urea as described previously (Jin *et al.,* 1994). RNA species were identified by staining with ethidium bromide in 0.5 M sodium acetate.

Northern blot analysis was performed essentially as described (Paterson *et al.,* 1984). Briefly, the RNA was fractionated on 1% agarose/formamide gels, blotted to a nylon membrane, and prehybridized with yeast tRNA (50 μg/ml) in hybridization buffer (50% formamide, 5× SSC, 1× Denhardt's solution, 0.1% SDS) at 42°C for 2 h. Riboprobes were generated by transcribing RNA from the indicated cDNAs cloned in pGEM3 using T_7 RNA polymerase in the presence of [^{32}P]-α-UTP (MaxiScript Kit, Ambion Inc., Austin, TX). [^{32}P]-labeled probes specific for 18S ribosomal RNA and influenza virus RNA segments encoding PA, PB1, PB2, or M proteins were hybridized to the membrane-immobilized RNA species followed by standard washes (Paterson *et al.,* 1984). Radioactivity was quantified by using a Fuji BioImager 1000 and MacBas software (Fuji Medical Systems, Stamford, CT).

Virus inactivation and multiplicity reactivation

Ultraviolet (UV) light-induced virus inactivation was performed by exposing allantoic fluid containing HA/NA and HAt−/NAt− viruses (0.5 ml/6-cm petri dish) to a 15 W UV light at a distance of 40 cm for the indicated times. The viruses were diluted serially and the virus infectivity titer determined by plaque assay (Paterson and Lamb, 1993).

Multiplicity reactivation was assayed by exposing 10^6 plaque-forming units (PFUs) of HA/NA or HAt−/NAt− to UV light for varying periods. The irradiated virus was used to infect 10^5 MDCK cells in 48-well tissue-culture plates for 1 h at 37°C. Cultures were washed with DMEM and incubated for 24 h at 37°C with DMEM containing 1 μg/ml *N*-acetyl trypsin. Cells were examined by microscopy and representative fields were photographed using a Nikon Diaphot (Nikon Corp., Tokyo, Japan) inverted microscope with phase contrast optics and a Kodak DCS 420 digital camera (Eastman Kodak Co., Rochester, NY).

Sucrose gradient ultracentrifugation

Monolayers of MDCK cells (10-cm plates) were infected with influenza viruses at a multiplicity of infection (m.o.i.) of 5–10 PFU/cell and at 4 h postinfection (hpi) cultures were incubated for 30 min with DMEM deficient in methionine and cysteine (DMEM met$^-$ cys$^-$). The cells were metabolically labeled with [^{35}S]Promix (100 μCi/ml; Amersham Pharmacia Biotech, Piscataway, NJ) for 12 h in 9 parts DME met$^-$ cys$^-$ and 1 part regular DMEM. The medium was harvested, clarified by low-speed centrifugation, and virions pelleted by centrifugation in a Beckman SW41 rotor (210,000 *g,* 1 h, 4°C). The virions were resuspended in NTE buffer and fractionated by velocity sucrose gradient centrifugation on a linear 20–50% sucrose gradient in a SW41 rotor (130,000 *g*, 1 h, 4°C). The gradients were fractionated from the top into 330-μl samples with a gradient fractionator (Auto Densi-Flow, Labconco Corporation, Kansas City, MO). Hemagglutinating activity of each fraction was measured (Paterson and Lamb, 1993) and the infectivity of each fraction was determined by plaque assay. Each fraction (250 μl) was precipitated with trichloroacetic acid (final concentration 10%) and virions recovered by centrifugation (15,000 *g*, 10 min). Polypeptides were boiled in SDS–PAGE sample buffer containing 2.5% (w/v) DTT, and separated on 15% polyacrylamide–SDS gels (Paterson and Lamb, 1993). Radioactivity was quantified using a Fuji BioImager 1000. Equilibrium sucrose gradient centrifugation of virions was performed using a linear 20–50% sucrose gradient in a Beckman SW41 rotor (130,000 *g*, 18 h, 4°C). The gradients were fractionated from the top and the amount of radioactivity in each fraction was quantified using a Beckman 7100 scintillation counter. The density of each fraction was determined by weighing a 100-μl sample of each fraction.

Electron microscopy

Electron microscopy was performed essentially as described previously (Jin *et al.,* 1997). Briefly, virions concentrated from pooled gradient fractions were diluted into NTE buffer containing a 1:500 dilution of polystyrene beads (5.8×10^{10} particles/ml) (Electron Microscopy Sciences, Inc., Fort Washington, PA) having an average diameter of 102 ± 3 nm. Diluted virions were allowed to absorb onto parlodion-coated copper grids for 30 s. Excess solution was wicked off and grids were negatively stained with 2% phosphotungstic acid, pH 6.6. A thin layer of carbon was evaporated onto the grids prior to examination of the grids in a Jeol JEM-100CX II electron microscope. For quantification, random fields of view were photographed at a magnification of 19,000×. The length and diameter of virions, and the number of polystyrene beads per field were determined directly from an examination of the negatives. A virion was considered elongated if its length was at least four times or greater than the average diameter of wt spherical influenza viruses.

Pseudotyping HAt−/NAt− virus with wt HA and NA

cDNAs encoding wt NA (Hiti and Nayak, 1982), wt HA (Sveda and Lai, 1981), and influenza virus C/Ann Arbor/1/50 HEF glycoprotein (Pekosz and Lamb, 1999) were

subcloned into the eukaryotic expression vector pCAGGS (Niwa *et al.,* 1991) and transfected into BHK cells using lipofectamine (Life Technologies, Gaithersburg, MD) according to the manufacturer's instructions. At 22 h posttransfection the cells were infected with HA/NA or HAt−/NAt− viruses (m.o.i. ~ 5 PFU/cell). At 3 hpi the cells were metabolically labeled with [^{35}S]Promix (100 μCi/ml) for 24 h in 3 parts DMEM met$^-$ cys$^-$ and 1 part regular DMEM. The medium was harvested, clarified by low-speed centrifugation, and virions pelleted by centrifugation in a Beckman SW41 rotor (130,000 *g,* 1 h, 4°C). The virions were resuspended in NTE buffer and fractionated by velocity sucrose gradient centrifugation on a linear 20–50% sucrose gradient in a Beckman SW41 rotor (130,000 *g*, 1 h, 4°C). Analysis of virion polypeptides was performed as described earlier.

ACKNOWLEDGMENTS

We thank Dr. Reay Paterson for constructing and making available the pCAGGS-HA plasmid. We thank all Lamb lab members for helpful discussions. This research was supported by Public Health Service research Grant R37 AI-20201 from the National Institute of Allergy and Infectious Diseases.

REFERENCES

Ada, G. L., Perry, B. T., and Abbot, A. (1958). Biological and physical properties of the Ryan strain of filamentous influenza virus. *J. Gen. Microbiol.* **19**, 23–39.

Ausubel, F. M., Brent, R., Kingston, R. E., Moore, D. D., Seidman, J. G., Smith, J. A., and Struhl, K. (1994). "Current Protocols in Molecular Biology, Vol. I and II." Wiley, New York.

Barry, R. D. (1961). The multiplication of influenza virus. II. Multiplicity reactivation of ultraviolet irradiated virus. *Virology* **14,** 398–405.

Blough, H. A. (1963). The effect of vitamin A alcohol on the morphology of myxoviruses. 1. The production and comparison of artificially produced filamentous virus. *Virology* **19,** 349–358.

Burnet, F. M., and Lind, P. E. (1957). Studies on filamentary forms of influenza virus with special reference to the use of dark-ground-microscopy. *Arch. ges. Virusforsch.* **7,** 413–422.

Cathomen, T., Naim, H. Y., and Cattaneo, R. (1998). Measles viruses with altered envelope protein cytoplasmic tails gain cell fusion competence. *J. Virol.* **72,** 1224–1234.

Choppin, P. W., Murphy, J. S., and Stoeckenius, W. (1961). The surface structure of influenza virus filaments. *Virology* **13,** 548–550.

Choppin, P. W., Murphy, J. S., and Tamm, I. (1960). Studies of two kinds of virus particles which comprise influenza A2 virus strains. III. Morphological characteristics: Independence of morphological and functional traits. *J. Exp. Med.* **112,** 945–952.

Colman, P. M. (1989). Neuraminidase: Enzyme and antigen. *In* "The Influenza Viruses" (R. M. Krug, Ed.), pp. 175–218. Plenum Press, New York.

Garcia-Sastre, A., and Palese, P. (1995). The cytoplasmic tail of the neuraminidase protein of influenza A virus does not play an important role in the packaging of this protein into viral envelopes. *Virus Res.* **37,** 37–47.

Hiti, A. L., and Nayak, D. P. (1982). Complete nucleotide sequence of the neuraminidase gene of human influenza virus A/WSN/33. *J. Virol.* **41,** 730–734.

Jin, H., Leser, G., and Lamb, R. A. (1994). The influenza virus hemagglutinin cytoplasmic tail is not essential for virus assembly or infectivity. *EMBO J.* **13,** 5504–5515.

Jin, H., Leser, G. P., Zhang, J., and Lamb, R. A. (1997). Influenza virus hemagglutinin and neuraminidase cytoplasmic tails control particle shape. *EMBO J.* **16,** 1236–1247.

Jin, H., Subbarao, K., Bagai, S., Leser, G. P., Murphy, B. R., and Lamb, R. A. (1996). Palmitylation of the influenza virus hemagglutinin (H3) is not essential for virus assembly or infectivity. *J. Virol.* **70,** 1406–1414.

Kilbourne, E. D., and Murphy, J. S. (1960). Genetic studies of influenza viruses. I. Viral morphology and growth capacity as exchangeable genetic traits. Rapid in ovo adaptation of early passage asian strain isolates by combination with PR8. *J. Exp. Med.* **111,** 387–406.

Lamb, R. A., and Krug, R. M. (1996). Orthomyxoviridae: The viruses and their replication. *In* "Fields Virology" (B. N. Fields, D. M. Knipe, and P. M. Howley, Eds.), 3rd ed., pp. 1353–1394. Lippincott-Raven Press, New York.

Luria, S. E., and Dulbecco, R. (1949). Genetic recombinations leading to productive active bacteriophage from ultraviolet inactivated bacteriophage particles. *Genetics* **34,** 93–125.

Mebatsion, T., Konig, M., and Conzelmann, K.-K. (1996). Budding of rabies virus particles in the absence of the spike glycoprotein. *Cell* **84,** 941–951.

Melikyan, G. B., Grener, S. A., Ok, D. C., and Cohen, F. S. (1997). Inner but not outer membrane leaflets control the transition from glycosylphosphatidylinositol-anchored influenza hemagglutinin-induced hemifusion to full fusion. *J. Cell Biol.* **136,** 995–1005.

Mitnaul, L. J., Castrucci, M. R., Murti, K. G., and Kawaoka, Y. (1996). The cytoplasmic tail of influenza A virus neuraminidase (NA) affects NA incorporation into virions, virion morphology, and virulence in mice but is not essential for virus replication. *J. Virol.* **70,** 873–879.

Niwa, H., Yamamura, K., and Miyazaki, J. (1991). Efficient selection for high-expression transfectants by a novel eukaryotic vector. *Gene* **108,** 193–200.

Nobusawa, E., Aoyama, T., Kato, H., Suzuki, Y., Tateno, Y., and Nakajima, K. (1991). Comparison of complete amino acid sequences and receptor-binding properties among 13 serotypes of hemagglutinin of influenza A viruses. *Virology* **182,** 475–485.

Paterson, R. G., Harris, T. J. R., and Lamb, R. A. (1984). Analysis and gene assignment of mRNAs of a paramyxovirus, simian virus 5. *Virology* **138,** 310–323.

Paterson, R. G., and Lamb, R. A. (1993). The molecular biology of influenza viruses and paramyxoviruses. *In* "Molecular Virology: A Practical Approach" (A. Davidson and R. M. Elliott, Eds.), pp. 35–73. IRL Oxford University Press, Oxford, UK.

Pekosz, A., and Lamb, R. A. (1999). Cell surface expression of biologically active influenza C virus HEF glycoprotein expressed from cDNA. *J. Virol.* **73,** 8808–8812.

Roberts, P. C., Lamb, R. A., and Compans, R. W. (1998). The M1 and M2 proteins of influenza A virus are important determinants in filamentous particle formation. *Virology* **240,** 127–137.

Rolls, M. M., Webster, P., Balba, N. H., and Rose, J. K. (1994). Novel infectious particles generated by expression of the vesicular stomatitis virus glycoprotein from a self-replicating RNA. *Cell* **79,** 497–506.

Schmitt, A. P., He, B., and Lamb, R. A. (1999). Involvement of the cytoplasmic domain of the hemagglutinin-neuraminidase protein in assembly of the paramyxovirus simian virus 5. *J. Virol.* **73,** 8703–8712.

Schnell, M. J., Buonocore, L., Boritz, E., Ghosh, H. P., Chernish, R., and Rose, J. K. (1998). Requirement for a non-specific glycoprotein cytoplasmic domain sequence to drive efficient budding of vesicular stomatitis virus. *EMBO J.* **17,** 1289–1296.

Sveda, M. M., and Lai, C.-J. (1981). Functional expression in primate cells of cloned DNA coding for the hemagglutinin surface glycoprotein of influenza virus. *Proc. Natl. Acad. Sci. USA* **78,** 5488–5492.